# Lasing characteristics of GaSb/GaAs self-assembled quantum dots embedded in an InGaAs quantum well

J. Tatebayashi,[a)] A. Khoshakhlagh, S. H. Huang, G. Balakrishnan, L. R. Dawson, and D. L. Huffaker[b)]
*Center for High Technology Materials, University of New Mexico, 1313 Goddard SE, Albuquerque, New Mexico 87106*

D. A. Bussian, H. Htoon, and V. Klimov
*Los Alamos National Laboratory, C-PCS MS J567, Los Alamos, New Mexico 87545*

(Received 26 February 2007; accepted 1 June 2007; published online 28 June 2007)

The authors report the optical characteristics of GaSb/GaAs self-assembled quantum dots (QDs) embedded in an InGaAs quantum well (QW). Variations in the In composition of the QW can significantly alter the emission wavelength up to 1.3 $\mu$m and emission efficiency. Lasing operation at room temperature is obtained from a 2-mm-long device containing five stacked GaSb QDs in $In_{0.13}Ga_{0.87}As$ QWs at 1.026 $\mu$m with a threshold current density of 860 A/cm$^2$. The probable lasing transition involves electrons and holes confined in the QW and QDs, respectively, resulting in a large peak modal gain of 45 cm$^{-1}$. A significant blueshift of the electroluminescence peak is observed with increased injection current and suggests a type-II band structure. © *2007 American Institute of Physics*. [DOI: 10.1063/1.2752018]

Quantum dots (QDs) in GaSb/GaAs materials are characterized by a staggered (type-II) band alignment, wide band gap range, and large valence band offset,[1,2] along with the zero-dimensional density of states (DOS).[3] In these materials, the electron is confined in the two-dimensional electronic gas (2DEG) formed by slight band bending at the GaSb/GaAs interface, while the hole is confined within the QD discrete energy levels. This unique collection of properties offers intriguing optoelectronic device possibilities on GaAs substrates including lasers, detectors, or solar cells. Moreover, type-II active region can be designed to work at a variety of wavelengths by varying the composition of the matrix surrounding the active region. Type-II quantum wells (QWs) have been shown to work very effectively in the mid-IR (Ref. 4) and type-II GaSb/GaAs QDs can be used for demonstrating similar results in the near-IR.[5–15] In addition, type-II QDs could be also useful for single carrier, even unipolar storage devices including optical memory[15] owing to their longer decay time [$\sim$10 ns (Refs. 7 and 9)].

Several groups have so far reported the optical properties of type-II GaSb QDs using the Stranski-Krastanov (SK) growth mode by molecular beam epitaxy[5–13] (MBE) or metal-organic chemical vapor deposition.[14,15] Our group has demonstrated high optical quality in both SK and interfacial misfit[16] (IMF) growth modes with photoluminescence (PL) indicating quantized energy levels and blueshift of the PL peak with increased pump power.[12] Moreover, the electroluminescence (EL) from GaSb IMF QDs at $\cong$1.3 $\mu$m has been demonstrated, which would be applicable to light sources in fiber-optic communication systems.[13] However, there have been no reports of type-II QD lasers, although many groups have demonstrated lasing from type-II QWs.[17] This is likely because the weak overlap of carrier wave function combined with QD-DOS is insufficient for high modal gain and lasing operations.

In this study, laser structures based on GaSb SK QDs in InGaAs QWs are fabricated for investigation. Samples are grown on (100) *n*-GaAs substrates by solid-state MBE followed by a 1.46 $\mu$m *n*-$Al_{0.3}Ga_{0.7}As$ clad, an active layer, a 1.46 $\mu$m *p*-$Al_{0.3}Ga_{0.7}As$ clad, and a 50 nm $p^+$-GaAs contact layer with a doping density of $2\times10^{19}$/cm$^3$. Si and Be are used as *n*- and *p*-type doping materials, respectively. The growth temperatures of *n* and *p* clads are 610 and 550 °C, respectively. The doping density of *n* or *p* clad is $2\times10^{17}$/cm$^3$ within 0.5 $\mu$m close to the waveguide and increases to $5\times10^{17}$/cm$^3$ for another 0.96 $\mu$m clad. The active layer consists of five stacked GaSb QDs in a 7 nm $In_{0.13}Ga_{0.87}As$ QW separated by 23 nm GaAs spacer, and is cladded by 90 nm GaAs. The growth rate, V/III ratio, and nominal thickness of QDs are 0.32 ML/s, 1, and 4 ML, respectively. The QD density is determined to be $3.0\times10^{10}$/cm$^2$ by atomic force microscope (AFM), as shown in Fig. 1(a). Figure 1(b) shows the cross-sectional transmission electron microscope (TEM) image indicating QDs embedded in the QW and sandwiched between GaAs buffer and cap. The width and height of QDs are estimated to be approximately 15 and 8 nm, respectively.

Figure 2 shows the room-temperature (RT) PL spectra of a single-layer GaSb QDs embedded in an $In_xGa_{1-x}As$ QW

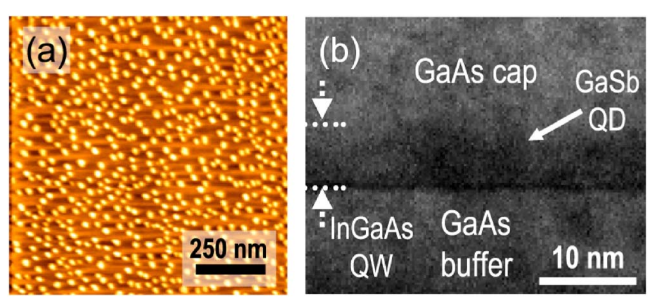


FIG. 1. (Color online) (a) AFM image of surface GaSb QDs (dot density: $3.0\times10^{10}$/cm$^2$). (b) Cross-sectional TEM image of GaSb QDs embedded in InGaAs QW.

[a)]Electronic mail: tatebaya@chtm.unm.edu
[b)]Electronic mail: huffaker@chtm.unm.edu

 

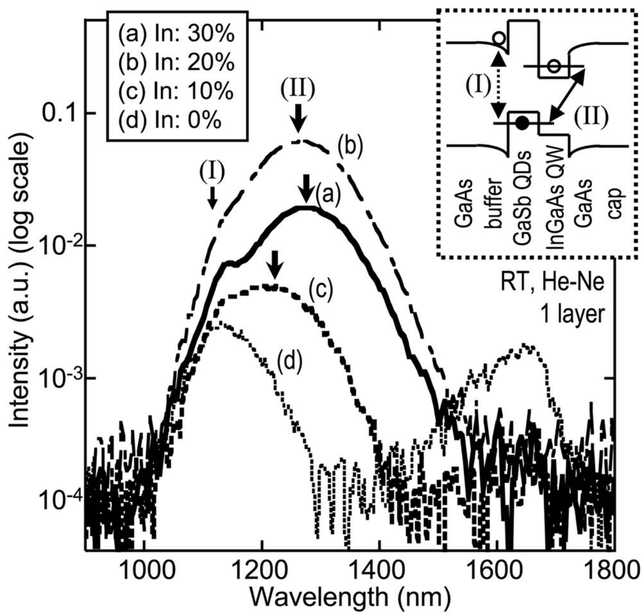


FIG. 2. RTPL spectra of a single-layer GaSb QDs embedded in $In_xGa_{1-x}As$ QW at various In composition of $x$. The inset is the schematic band diagram of GaSb QDs embedded in InGaAs QW.

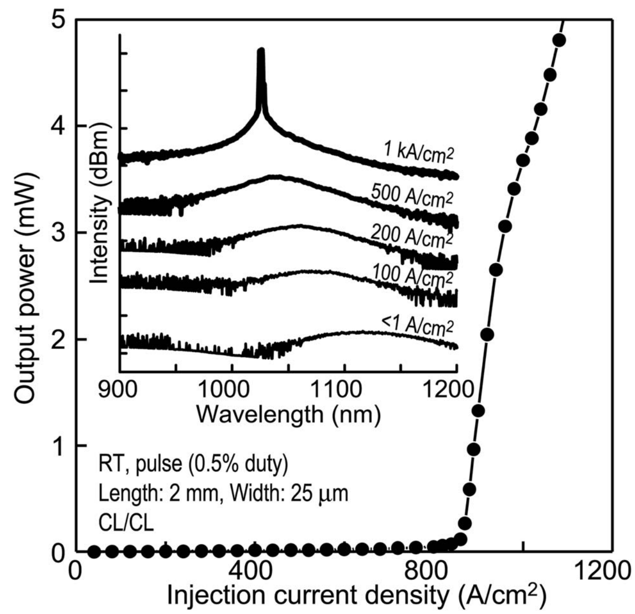


FIG. 3. $L$-$I$ characteristics of a 2-mm-long device containing five-stacked GaSb QDs in $In_{0.13}Ga_{0.87}As$ QW. The solid line is a guide for the eyes. A threshold current density $J_{th}$ is 860 A/cm$^2$. The inset is the EL spectra of the 2-mm-long laser ranging from <1 A/cm$^2$ to 1 kA/cm$^2$.

with different In compositions ($x$) with an excitation by a 5 mW He–Ne laser with a 1.5 mm spot size. The $W$ configuration of the inset of Fig. 2 illustrates the likely band structure for the GaSb/InGaAs ensemble showing a large conduction band offset formed by the QW for effective electron confinement while holes are confined within QDs. Such a band structure results in both increased electronic DOS and increased electron confinement to provide high gain despite of the type-II band alignment. Two most probable electronic transitions are labeled (I) and (II). Transition (I) indicates an electron confined in a 2DEG at the GaAs/GaSb interface. Transition (II) includes a more strongly confined electron in the QW surrounding QDs. Transition (II) is more probable compared to (I) and results in a longer wavelength emission. The PL spectra in Fig. 2 show the existence of two peaks: one peak at 1.13 $\mu$m, and another peak at 1.205, 1.265, or 1.28 $\mu$m from the samples with $x$=0.1, 0.2, or 0.3, respectively. The first steady peak at 1.13 $\mu$m is the same as those measured from GaSb QDs capped with GaAs (Ref. 12) and likely due to transition (I) processes. The second peak probably results from transition (II) processes. The increased In composition in the QW reduces the band gap of the QW resulting in an increased electron confinement, subsequent intensity increase, and a longer emission wavelength. It is noted that a carrier decay time >8 ns at RT or 40–70 ns at 4 K is measured for the same GaSb/GaAs QDs in InGaAs QW, whose detailed study will be reported somewhere.

Broad area edge emitters (25-$\mu$m-wide stripe) are fabricated by conventional device processing with as-cleaved facets on both sides. Cavity lengths ($L_c$) range from 0.5 to 5 mm. All measurements are performed under pulsed conditions with a pulse width of 500 ns and 0.5% duty cycle. The EL spectra and output power-current ($L$-$I$) characteristics are collected by multi mode optical fiber and detected by an optical spectrum analyzer and Ge optical powermeter, respectively. Figure 3 shows the $L$-$I$ curve and EL spectra at current densities ($J$) ranging from <1 A/cm$^2$ to 1 kA/cm$^2$ for $L_c$=2 mm. The RT lasing at 1.026 $\mu$m is obtained with the threshold current density ($J_{th}$) of 860 A/cm$^2$ with a peak output power of >5 mW at 1.1 kA/cm$^2$. The EL emission from GaSb QDs shown in the inset of Fig. 3 emerges at the initial wavelength of 1.12 $\mu$m with $J$<1 A/cm$^2$ and shifts towards shorter value to ≅1.02 $\mu$m at $J$=1 kA/cm$^2$ indicating a total blueshift of ~100 nm. The shorter peak wavelength of 1.12 $\mu$m measured from the devices compared to the RTPL study peaked at 1.21 $\mu$m likely results from Sb intermixing into the InGaAs matrix during upper clad growth at ~550 °C.

Lasing parameters are analyzed from a collection of devices with varied $L_c$ from 0.5 to 5.0 mm. These data, which include lasing wavelength ($\lambda_{pk}$), $J_{th}$, external quantum efficiency ($\eta_{ext}$), and peak modal gain ($G_{pk}$) at $J_{th}$, are listed in Table I. $\lambda_{pk}$ and $J_{th}$ vary with $L_c$ and range from 1.016 $\mu$m at 1.4 kA/cm$^2$ to 1.033 $\mu$m at 0.68 kA/cm$^2$ for $L_c$=0.5 and

TABLE I. Lasing peaks ($\lambda_{pk}$), threshold current densities ($J_{th}$), external quantum efficiency ($\eta_{ext}$), and peak modal gain at $J_{th}$ (threshold modal gain, $G_{th}$) of 25-$\mu$m-width devices with different cavity lengths ($L_c$).

| $L_c$ (cm) | 0.05 | 0.1 | 0.15 | 0.2 | 0.3 | 0.4 | 0.5 |
|---|---|---|---|---|---|---|---|
| $\lambda_{pk}$ (nm) | 1016 | 1020 | 1025 | 1026 | 1028 | 1030 | 1033 |
| $J_{th}$ (A/cm$^2$) | 1402 | 1136 | 893 | 863 | 783 | 687 | 678 |
| $\eta_{ext}$ | 0.23 | 0.12 | 0.089 | 0.052 | 0.048 | 0.037 | 0.032 |
| $G_{th}$ (cm$^{-1}$) | 44.8 | 33.4 | 29.6 | 27.7 | 25.8 | 24.8 | 24.3 |

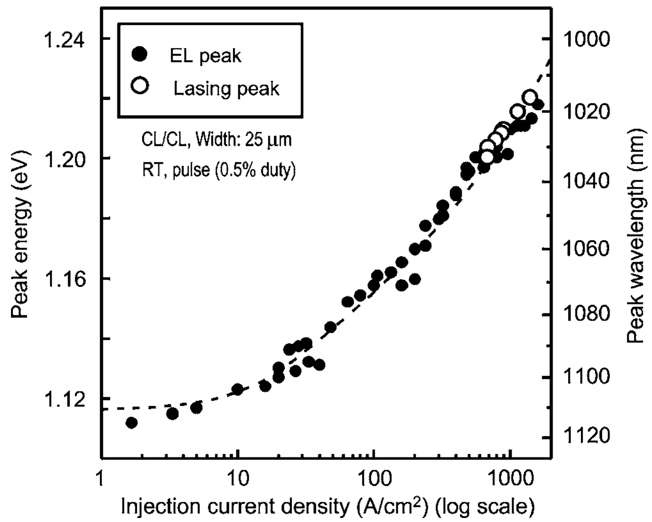


FIG. 4. EL (closed circle) and lasing (open circle) peak energy of the fabricated device versus injection current densities ($J$). The dashed line is a fit to the third root of $J$.

5 mm, respectively. These $\lambda_{pk}$ are longer than those of InGaAs QW lasers (0.98 $\mu$m) (Ref. 18) with the same In composition and thickness. The transparent current density, $J_\infty$ $=106$ A/cm$^2$ per QD layer, can be derived by extrapolating the $J_{th}$ to zero optical loss from the relation between $J_{th}$ and $L_c$. This somewhat high value, compared to InAs QD lasers ($\sim 10$ A/cm$^2$ per layer), can be attributed to the reduced overlap of the matrix element characteristics of the possible type-II band alignment. $\eta_{ext}$ also varies with $L_c$ and ranges from 0.22 to 0.032. We calculate the internal loss, $\alpha_i$ $=22$ cm$^{-1}$, by plotting the inverse $\eta_{ext}$ as a function of $L_c$. $\alpha_i$ is somewhat high for QD lasers but comparable to QW lasers. $G_{pk}$ as a function of $J=J_{th}$ is determined by the expression $G_{pk}=G_{th}=\alpha_i+\ln(1/R_1R_2)/2L_c$, where $G_{th}$ is a threshold modal gain and $R_{1(2)}=0.32$ is a facet reflectivity. Proportional increase in $G_{pk}$ can be observed from 24.3 cm$^{-1}$ for $L_c$ $=5.0$ mm to 44.8 cm$^{-1}$ for $L_c=0.5$ mm, which shows different characteristics from InAs QD lasers where the modal gain is saturated by increasing $J$.[19] $G_{pk}$ is larger than that of InAs QD lasers which are typically $\sim 20$ cm$^{-1}$ for five to ten stack QDs. This larger $G_{pk}$ could result from electron confinement within the QW-DOS rather than the QD-DOS.

Figure 4 plots the detailed dependence of EL peak energy ($E$) (closed circle), along with $\lambda_{pk}$ (open circle) for the lasers with different $L_c$ just above threshold. A dashed line shows a fit to the third root of $J$ for the comparison with the PL blueshift by increased pump powers.[5,8,9] This $E$-$J$ curve indicates that the shift of the EL peak defined by $dE/dJ$ is significant at lower currents [$dE/dJ \sim 0.17$ meV/(A/cm$^2$)], but the blueshift clamps at higher $J$ above $\cong 500$ A/cm$^2$ ($dE/dJ \sim 0.022$). The $\lambda_{pk}$ with different $L_c$ appear at the saturated region of the $E$-$J$ curve lying above $\cong 500$ A/cm$^2$. The clamping of the EL blueshift might be due to a saturation of hole energy levels in the finite QD-DOS. An alternative reason for the blueshift could be Sb intermixing into GaAs matrices resulting in type-I band alignment[20] and subsequent band filling at higher values of $J$. However, the clamping of the blueshift is associated more closely with type-II transitions, as described by Hatami *et al.*,[9] than with the band-filling effect. Furthermore, the clamping of blueshift is also seen for type-II GaAsSb QW lasers which show initial $dE/dJ$ of $\cong 1.2$ and a final lasing value of $\cong 0.12$.[21] The smaller values of $dE/dJ$ for the QDs compared to type-II QWs for both low and high $J$ are likely due to the stronger hole confinement within the finite QD-DOS compared to the infinite QW-DOS.

In summary, we report the optical characteristics of GaSb/GaAs QDs embedded in InGaAs QW. Variations in the In composition of InGaAs QW can significantly alter the emission wavelength up to 1.3 $\mu$m. Lasing operation at RT is obtained from five stacked GaSb QDs in $In_{0.13}Ga_{0.87}As$ QW ($J_{th}=860$ A/cm$^2$) at $\lambda_{pk}=1.026$ $\mu$m with $L_c=2$ mm. Our rationale is shown towards a probable type-II lasing transition involving electrons and holes confined in the QW and QDs, respectively. A longer $\lambda_{pk}$ than InGaAs QW lasers, a larger $G_{pk}$ of 45 cm$^{-1}$ compared to InAs QD lasers, and a significant blueshift ($\cong 100$ nm) of the EL peak with increased $J$ further support this theory.

This work is supported by the Air Force Office of Scientific Research (FA9550-06-1-0407) under Gernot Pomrenke and Kitt Rheinhardt. The authors would like to thank A. Albrecht and M. Mehta for their support of laser characterization.

[1] G. A. Sai-Halasz, L. L. Chang, J. M. Welter, C. A. Chang, and L. Esaki, Solid State Commun. **27**, 935 (1978).
[2] H. Kroemer and G. Griffiths, IEEE Electron Device Lett. **EDL-4**, 20 (1983).
[3] Y. Arakawa and H. Sakaki, Appl. Phys. Lett. **40**, 932 (1982).
[4] J. R. Meyer, C. A. Hoffman, F. J. Bartoli, and L. R. Ram-Mohan, Appl. Phys. Lett. **67**, 757 (1995).
[5] F. Hatami, N. N. Ledentsov, M. Grundmann, J. Bohrer, F. Heinrichsdorff, M. Beer, D. Bimberg, S. S. Ruvimo, P. Werner, U. Gosele, J. Heydenreich, U. Richter, S. V. Ivanov, B. Y. Meltser, P. S. Kop'ev, and Z. I. Alferov, Appl. Phys. Lett. **67**, 656 (1995).
[6] B. R. Bennett, B. V. Shanabrook, and R. Magno, Appl. Phys. Lett. **68**, 958 (1996).
[7] C.-K. Sun, G. Wang, J. E. Bowers, B. Brar, H.-R. Blank, H. Kroemer, and M. H. Pilkuhn, Appl. Phys. Lett. **68**, 1543 (1996).
[8] E. R. Glaser, B. R. Bennett, B. V. Shanabrook, and R. Magno, Appl. Phys. Lett. **68**, 3614 (1996).
[9] F. Hatami, M. Grundmann, N. N. Ledentsov, F. Heinrichsdorff, R. Heitz, J. Böhrer, D. Bimberg, S. S. Ruvimov, P. Werner, V. M. Ustinov, P. S. Kop'ev, and Zh. I. Alferov, Phys. Rev. B **57**, 4635 (1998).
[10] K. Suzuki, R. A. Hogg, and Y. Arakawa, J. Appl. Phys. **85**, 8349 (1999).
[11] I. Farrer, M. J. Murphy, D. A. Ritchie, and A. J. Shields, J. Cryst. Growth **251**, 771 (2003).
[12] G. Balakrishnan, J. Tatebayashi, A. Khoshakhlagh, S. H. Huang, A. Jallipalli, L. R. Dawson, and D. L. Huffaker, Appl. Phys. Lett. **89**, 161104 (2006).
[13] J. Tatebayashi, A. Khoshakhlagh, S. H. Huang, L. R. Dawson, G. Balakrishnan, and D. L. Huffaker, Appl. Phys. Lett. **89**, 203116 (2006).
[14] M. Motlan and M. E. Goldys, Appl. Phys. Lett. **79**, 2976 (2001).
[15] M. Geller, C. Kapteyn, L. Müller-Kirsch, R. Heitz, and D. Bimberg, Phys. Status Solidi B **238**, 258 (2003).
[16] A. M. Rocher, Solid State Phenom. **19/20**, 563 (1991).
[17] E. Lugagne-Delpon, P. Voisin, M. Voos, and J. P. André, Appl. Phys. Lett. **60**, 3087 (1992).
[18] D. J. Arent, K. Deneffe, C. Van Hoof, J. De Boeck, and G. Borghs, J. Appl. Phys. **66**, 1739 (1989).
[19] L. V. Asryan and R. A. Suris, IEEE J. Sel. Top. Quantum Electron. **3**, 148 (1997).
[20] A. D. Prins, D. J. Dunstan, J. D. Lambkin, E. P. O'Reilly, A. R. Adams, R. Pritchard, W. S. Truscott, and K. E. Singer, Phys. Rev. B **47**, 2196 (1993).
[21] W. W. Chow, O. B. Spahn, H. C. Schneider, and J. F. Klem, IEEE J. Quantum Electron. **37**, 1178 (2001).